Visualization of TiO_2 reduction behavior in molten salt electrolysis

Shungo Natsui[1,2*], Takuya Sudo[1], Ryota Shibuya[1], Hiroshi Nogami[2], Tatsuya Kikuchi[1], and Ryosuke O. Suzuki[1]

1 Division of Materials Science and Engineering, Faculty of Engineering, Hokkaido University, Kita 13 Nishi 8, Kita–ku, Sapporo, 060–8628 Japan.

2 Institute of Multidisciplinary Research for Advanced Materials, Tohoku University, 2-1-1 Katahira, Aoba-ku, Sendai 980-8577, Japan.

(Present affiliation of first author is [2]Tohoku University)

* Corresponding author.

E-mail: natsui@tohoku.ac.jp

Tel.: +81–22–217–5157

Abstract:

An in-situ observation technique of the TiO_2 interfacial behavior in molten LiCl-KCl electrolysis was developed. The variation of the thin TiO_2 electrode surface were tracked through the high-speed digital microscopy synchronized with the electrochemical measurement. Two characteristic interfacial behaviors were discovered: physical breakage of the titanium oxide and Li(*l*) spreading on electrode surface. These electrochemically induced interfacial behaviors affect the current-time curves due to the heterogeneity of the titanium oxide film shape.

Keywords:

Molten salt electrolysis; Titanium oxide; High-speed microscopy; LiCl-KCl; Liquid Li;

In the refining industries of the oxide-stable metallic elements, the electrolysis of the molten chloride is indispensable. Thus, and efficient electrolysis has been developed, for example, for use in the Kroll process for titanium production. In the Kroll process, TiO_2 is first converted to $TiCl_4$ by Cl_2 gas. Then, liquid Mg reduces the $TiCl_4$ such that high-purity metallic sponge Ti is obtained. The liquid Mg and gaseous Cl_2 are regenerated by electrolysis of the byproduct $MgCl_2$ and recycled.

In order to avoid some complicated steps in the Kroll process, the direct electrochemical decomposition of TiO_2 in molten $CaCl_2$ has been proposed. In the FFC Cambridge process, the oxide anion cathodically transfers from the solid TiO_2 pellet to the anode in a molten salt bath.[1] Because the Ti-O binary system contains many suboxides, oxygen in the higher oxide is removed to form a lower oxide upon receiving an electrical charge from the cathode.

Another promising method, the OS process, has been proposed, in which the oxide anion transfer in $CaCl_2$ is better utilized because as much as 20 mol% CaO that acts as an electrolyte can dissolve into the molten $CaCl_2$ at 1173 K[2-5]. The electrochemically deposited, liquid Ca at the cathode also dissolves into the molten $CaCl_2$, and the dissolved Ca works effectively to reduce the titanium oxide powder. Similarly, LiCl and its binary chloride systems can dissolve oxygen anions at lower temperatures,[6-8] and KCl is sometimes added to lower the

temperature further.[9] Electrochemically deposited liquid Li in molten LiCl-KCl has been observed to form droplets on an attached cathode.[10] Despite its importance, there is only limited knowledge about the dynamic reducing behavior of TiO_2 by liquid Li. Recently, black, film-like, colloidal Li (in the form of a metal fog) was observed on an electrodeposited thin Li metal in molten LiCl-KCl.[11] The detailed behavior of reducing TiO_2 ,however, has yet to be clarified.

A detailed understanding of the dynamic behavior of TiO_2 reduction is necessary to control and optimize the electrolysis. Besides improving the FFC and OS processes, such knowledge can be applied immediately to the current molten salt electrolysis processes and would bring a large energy savings due to increased thermal efficiency in the metal-refining industries. Cyclic voltammograms (CVs) of the oxide electrode in high-temperature molten salts display unique features that the reduction current including multi-interfacial transient dynamic behavior [12]. Data on the reduction rate, current efficiency, and energy consumption during the electroreduction of oxides under potentiostatic conditions were recorded, and these experimental findings form the basis of the optimization of the electroreduction method [13, 14]. For an in-depth discussion, we developed an in-situ observation technique to observe the TiO_2 interfacial behavior in molten LiCl-KCl electrolysis by tracking the thin fine TiO_2 electrode surface obtained by the high-speed

digital microscopy synchronized with the electrochemical measurement in this study.

A schematic diagram of the experimental apparatus is depicted in a reference.[10, 15] A vertical quartz glass vessel with a barrel-vaulted (semicylindrical) shape, 100 mm in diameter and 250 mm in height, (Kondo Science, Inc.) was employed. The flat side of the vessel enabled in-situ observations. An electric resistance furnace (SiC heater) with a flat quartz window was designed to observe the phenomena within the vessel under controlled temperature. A metal halide light (Photron Co., Ltd., HVC-SL, maximum light flux: 12,500 lm) was used as an auxiliary light source.

Changes in the electrode interface were recorded at a rate of 500 fps (0.002 s intervals) with the image size of 640 × 480 pixels using a high-speed digital camera (Ditect Co., Ltd., HAS-D71, monochrome). With a long-distance zoom lens (VS Technology Co. Ltd., VSZ-10100, working distance: 95 mm), the minimum field of view is 666 μm × 500 μm and the maximum resolution of 1.04 μm was obtained. The electrode surface morphology was tracked in each captured image by image processing software (Photron Co., Ltd., PFV Viewer). Reagent-grade LiCl (Wako Pure Chemical Co. Ltd., >99.0%) and KCl (Wako, >99.5%) were used for preparing the melt.

The eutectic mixture of LiCl–KCl (59:41 mol%, melting point = 625 K (352 ºC)) was packed in a borosilicate glass crucible with a flat side was settled in the vessel and was dried in vacuum at 573 K (300 ºC) for more than 12 h. Then it was heated up to 673 K (400 ºC, the constant

112 experimental temperature) and maintained for 5 h to remove residual
113 water. All experiments were conducted in an Ar atmosphere
114 (>99.9995%). The melt temperature was measured with a K-type
115 thermocouple with a glass sheath.

116 After the mixed salt was melted, the suspended electrodes were
117 immersed into the melt. Three types of working electrode were
118 prepared from Ti rod (Nilaco Corp., ϕ 1.5 mm, 99.5%). First was as
119 received, second and third were heat-treated for 1 h under 1073 and
120 1173 K, respectively. **Figure 1 (a)** shows the appearances of prepared
121 titanium oxide electrodes. On the surface of the heat-treated electrodes,
122 a white oxide film formed on each. The scanning electron microscope
123 (SEM) image shown in Fig. 1(b) clearly showed the formation of oxide
124 film on the surface of the electrode, and the X-ray diffraction (XRD)
125 pattern of the fabricated electrode (Fig. 1 (c)) identified the oxide film
126 as mainly TiO_2. The average thicknesses of the oxide films obtained
127 from the SEM images increased with the heat-treatment temperature,
128 namely 0.0, 2.0 and 7.3 μm; thus, the three samples were named T0.0,
129 T2.0 and T7.3. The immersion depth of the working electrode was fixed
130 at 40 mm and the other part of the electrodes was insulated using
131 protective Al_2O_3 tube as shown in Fig. 1 (a). The counter electrode was
132 a graphite rod (Toyo Carbon Corp., ϕ 10 mm). An Ag^+/Ag reference
133 electrode was employed. This electrode, consisted of a silver wire (ϕ
134 1.0 mm, 99.99%, Nilaco), a LiCl-KCl eutectic melt containing 0.5
135 mol% AgCl (Wako, 99.5%) and a borosilicate tube, and the silver wire
136 was immersed in the eutectic melt within the tube. Electrochemical

137 measurements were performed using an automatic polarization system
138 (Hokuto Denko Corp., HZ-5000). The inter-electrode voltage and
139 microscope images were synchronized with an error less than 4 μs by
140 using an analogue signal synchronous system (Ditect Co., Ltd., DI-
141 SYNC 29N).

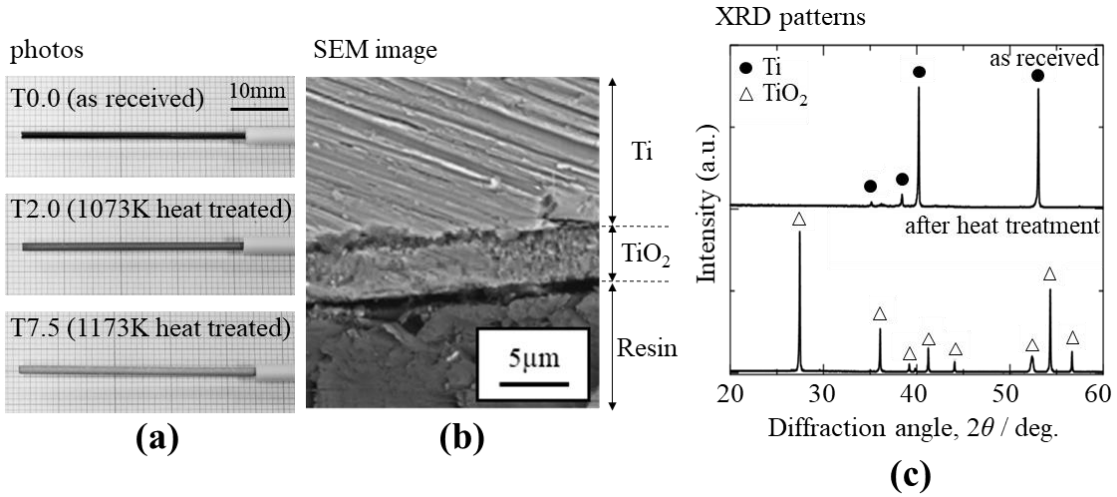

142 Fig. 1 Titanium oxide electrode previously prepared by heat treatment under air environment. (a):
143 Photos of the three, different-thickness titanium oxide electrodes. (b): Scanning electron microscope
144 (SEM) image of the T2.0 electrode cross-section. (c): X-ray diffraction (XRD) pattern of electrodes
145 before and after heat treatment.

146

147 **Figure 2** shows the cyclic voltammogram (CV, scan rate: 10 mV /
148 s) obtained by the T7.5 working electrode. Sharp increases in the
149 cathodic and corresponding anodic currents compared to the Ag/Ag^+
150 reference electrode were observed at about E = −2.4 V. These two
151 current changes are thought to be due to the deposition of Li(*l*) and
152 the dissolution of the deposits, respectively.[16] The cathodic current
153 at E = −0.7 to −1.0 V is the reported reduction potential of the

titanium ion: $Ti^{4+} + e^- \rightarrow Ti^{3+}$ (E = −0.9 V); $Ti^{3+} + e^- \rightarrow Ti^{2+}$ (E = −1.0 V).[17] Although the solubility of Li_2O was estimated to be 0.31 mol% in LiCl-KCl eutectic melt at 673 K (400 ºC) [8], because of the negligible solubility of TiO_2, the direct electrochemical reduction of the TiO_2 following the mechanism of the FFC process described in Eq. 1.

$$TiO_x + e^- \rightarrow TiO_{x-1} + \frac{1}{2}O^{2-} \quad (1)$$

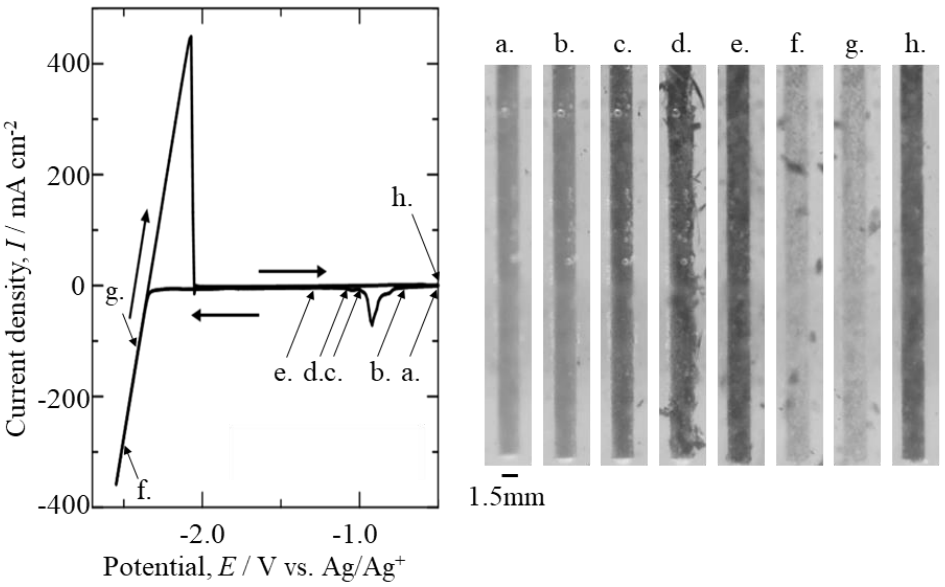

Fig. 2. Cyclic voltammogram and corresponding photographs of T7.5 titanium oxide electrode in LiCl-KCl. Images were taken at a: -0.50V, b: -0.70V, c: -1.00V, d: -1.10V, e:-1.30V, f:-2.50V, g: -2.45V, h: -0.50V.

With the progress of potential, the appearance of the TiO_2 electrode changed from white to black as shown in the photos in Fig. 2a-c. Fig. 2d showed the breakage of the black surface, and small

168 pieces broke apart from the electrode. At this moment, the current
169 density became approximately zero, and thus the reactivity of the
170 electrode surface was lost due to mechanical disconnection. In the
171 initial stage of potential progression, the deformation of the titanium
172 oxide occurred due to the volume change with the electrochemical
173 reduction. Next, the deformed part of the surface was partially peeled
174 off from the electrode and dispersed into the melt. In Fig. 2f-g, no
175 metal fog was observed in the Li(l) electrodeposition while only silver
176 white precipitate was observed. According to a previous study [10],
177 when an inactive Mo electrode was used as the working electrode, a
178 blue metal fog was generated, and the amount of the fog generation
179 decreased as the amount of oxide ions increased. The metal fog is also
180 related to the amount of Li(l) and the time of the dissolution; however,
181 it was likely that the oxide ions already existed in the vicinity of the
182 working electrode due to the titanium oxide reduction.

183 The ratio of the electric charges passing through the anode to
184 one through the cathode, (q_a/q_c), in the region of E < -2.0V gave a
185 momentary coulombic efficiency of $q_a/q_c = 0.871$. This showed that the
186 precipitation of the Li(l) advanced the cathodic reaction of the Ti oxide
187 by the OS process mechanism as described by Eq. 2:

$$Li^+ + e^- \rightarrow Li(l) \quad (2a)$$

$$TiO_y + 2Li(l) \rightarrow TiO_{y-1} + Li_2O(\text{dissolved}) \quad (2b)$$

188 In the CV measurement, mechanical deformation of titanium oxide

occurs during the potential sweep, so it is difficult to know the behavior of the TiO_2 electrode that corresponds to the Li(*l*) electrodeposition potential.

Figure 3 shows the behavior of the TiO_2 electrode surface obtained by the high-speed observation during the chronoamperometry measurement under -2.75 V for 2.000s. (See also the electronic supplementary video files for more detailed understanding. Each video is 6 seconds long.)

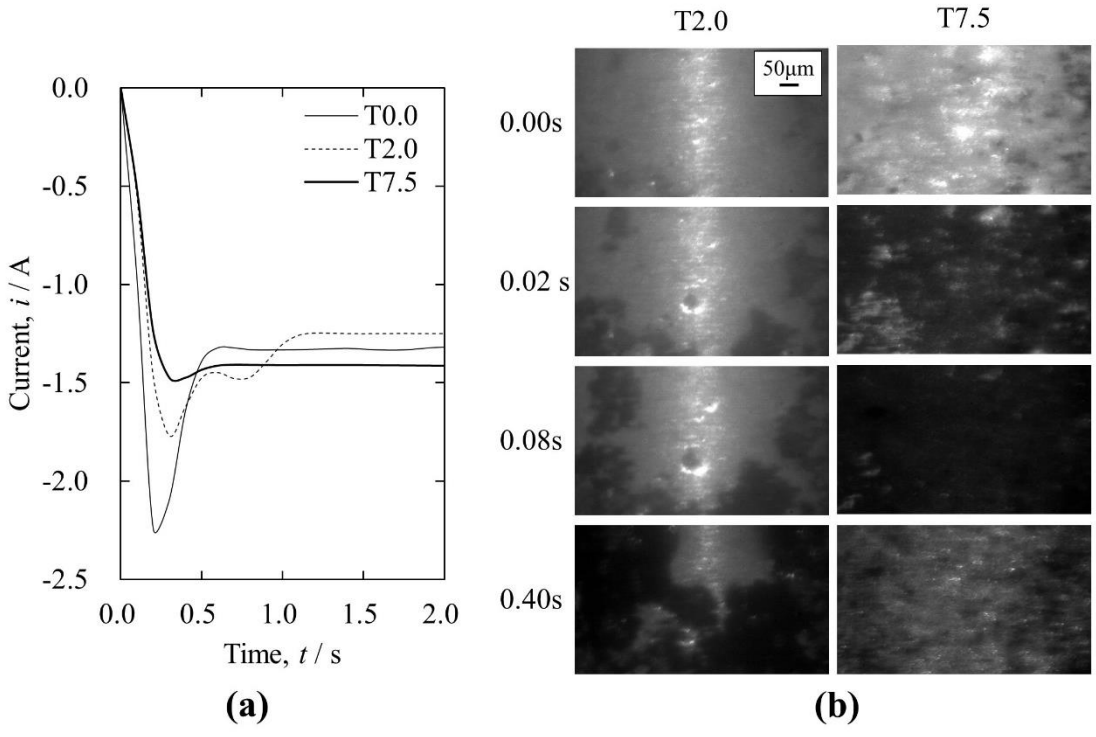

Fig. 3. Electro-reduction behavior of T2.0 and T7.3 TiO_2 electrodes observed by chronoamperometry (at E = -2.75 V). (a): current-time curves, (b): representative photographs of electrode.

After the initial increase, the current converged to the approximately constant value in all samples. The initial peak current was the largest at T0.0 and showed a tendency to decrease as the TiO_2 film thickness

increased. The surface of the T2.0 electrode changed from white to black immediately after the application of potential. This change proceeded non-uniformly and showed mottled pattern grown from black spots. The black part was the titanium oxide reduced by the mechanism of Eq. 1 (or perovskites like $LiTiO_2$ and $LiTi_2O_4$ [18]). After the electrolysis at a constant potential, the black-colored titanium oxide surface was also observed in the CV test.

In the case of the T7.5 electrode, the black surface rapidly developed, and it became uniform as electrochemical reduction progressed. After t = 0.08 s, the metallic droplets formed, and the metallic liquid spread onto the cathode surface. This phenomenon indicated that the reduction reaction of the TiO_x was progressing by the electrochemical deposition mechanism of Eq. 2a and 2b. After t = 2.0 s, all metallic droplets disappeared, and the black titanium oxide surface remained. To understand in detail the transient change in the TiO_x structure, our future work will involve the chemical analysis of the sample.

From the differences in behaviors of the T2.0 and T7.5 electrodes, the following conclusions can be drawn. For the initial TiO_2 with a high electric resistance, the reduction proceeds by the mechanism of Eq. 1 and the conductivity increases; this reaction should grow heterogeneously on the cathode surface. Therefore, after Li(l) generated in a region having a relatively high conductivity on the cathode surface, the reaction progresses by spreading over the surface of the electrode. The T7.5 sample has not only thicker but also more porous TiO_2 layer than the T2.0 film.[19,20] The reduction of film TiO_2

229 did not damage the electrolytic product because of the presence of the
230 electrochemical reaction interface, i.e. highly conductive Li (*l*) and
231 molten salt, on the oxide film. Thus, before electrolysis, the molten
232 salt penetrates into the inside of the porous TiO_2, and the generated
233 Li(*l*) droplet causes a lower electrical resistance. The reduction of
234 titanium oxide on the surface progresses by Eq. 2 to wet Li(*l*) on the
235 entire electrode surface.

236 Figure 4 shows the voltage behavior between WE and CE, *U*, and the
237 observed T2.0-TiO_2 electrode surface under various potentials for
238 2.000 s. At *E* = -1.0 V, *V* became almost constant and showed a
239 maximum at *t* = 0.08 s, but *V* at *E* = -1.5, -2.0, and -2.5 V showed
240 unstable behaviors. As seen in the figure, the color of each electrode
241 changed to black after the potential was applied. However, when TiO_x
242 broke locally as shown in Fig. 2, the electrical conductivity of the
243 electrode became non-uniform. This is the probable reason for voltage
244 fluctuations. When *E* = -2.75 V, some shiny parts that appear to be Li(*l*)
245 are found at *t* = 1.90 s. Here, Eq. 1 was the dominant reaction initially,
246 but Eq. 2 was dominant on some parts of the electrode surface. Once
247 Li(*l*) is formed, it becomes the current-carrying site and Eq. 2 proceeds
248 further.

249 Summarizing, a system was constructed to visualize titanium oxide
250 reduction based on molten salt electrolysis in order to better
251 understand its representative interfacial behavior in this study. We
252 focused on reducing TiO_2 in molten LiCl-KCl eutectic salt at 673 K.
253 The observed characteristic interfacial behaviors include (1)

mechanical breakage of titanium oxide by the electrochemical reduction and dispersion of titanium oxide into the bath, (2) local electrochemical reductions at the conductive regions, due to surface nonuniformity, and (3) electrodeposited Li(*l*) wetting the titanium oxide during the reduction reaction. The results from both the cathode interfacial snapshots and the current-time curves suggest that it is important to increase the area of the reactive region between the titanium oxide and the molten salt for efficient reduction by electrodeposited Li(*l*) by avoiding a concentration of Li(*l*).

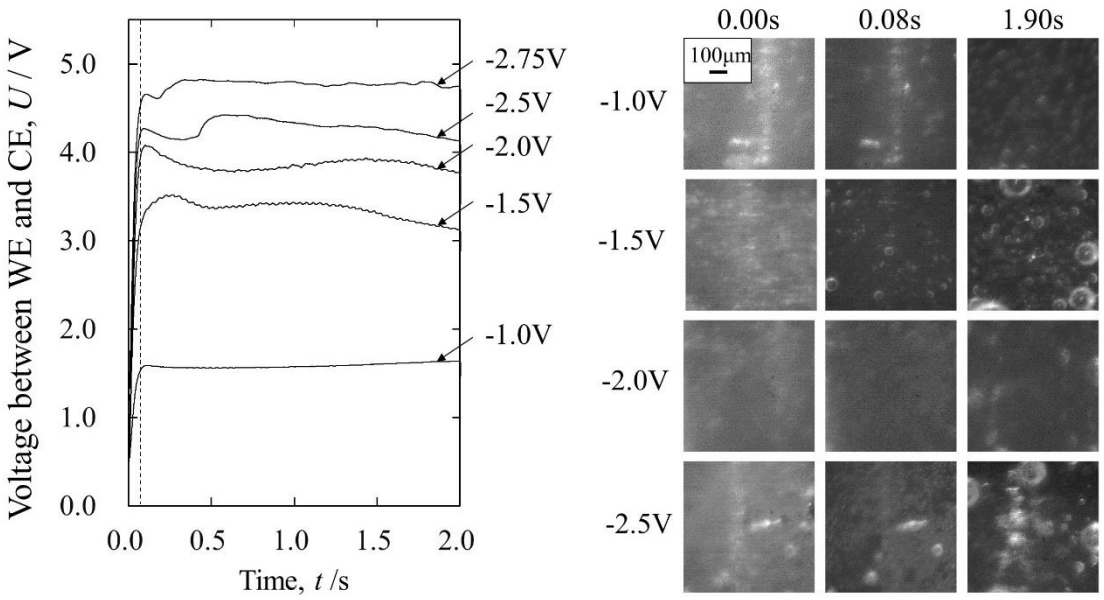

Fig. 4. Electro-reduction behavior of T2.0 TiO_2 electrodes observed by chronoamperometry (at various potentials). (a): voltage-time curves, (b): representative photographs of electrode.

This work was made possible by the financial support from the Grant-in-Aid for Scientific Research (KAKENHI grant no. 18K14036), the

Iketani Science and Technology Foundation (grant no. 0291073-A), Tanikawa Fund Promotion of Thermal Technology, and Amano Institute of Technology.

REFERENCES

1) G. Z. Chen, D. J. Fray and T. W. Farthing: *Nature*, 2000, vol. 407, pp. 361–64.

2) K. Ono, and R. O. Suzuki: *JOM*, 2002, vol. 54, pp. 59–61.

3) R. O. Suzuki, and S. Inoue, *Metall. Mater. Trans. B*, 2003, vol. 34, pp. 277–85.

4) R. O. Suzuki, H. Noguchi, H. Hada, S. Natsui, and T. Kikuchi: *Mater. Trans.*, 2017, vol. 58, pp. 341–349.

5) H. Noguchi, S. Natsui, T. Kikuchi, and R. O. Suzuki: *Electrochem.*, 2018, vol. 86, pp. 82–87.

6) J. M. Hur, S. C. Lee, S. M. Jeong, and C. S. Seo: *Chem. Lett.*, 2007, vol.36, pp.1028-29.

7) M. W. Lee, E. Y. Choi, S. C. Jeon, J. Lee, S. B. Park, S. Paek, M. F. Simpson, S. M. Jeong: *Electrochem. Commun.*, 2016, vol. 72, pp.23-26.

8) Y. Sakamura: *J. Electrochem. Soc.*, 2010, vol. 157, pp. E135–E139.

9) Y. Katayama and B. Friedrich: *Electrochem. Soc. Proc.*, 2004, vol. 2004, pp. 1046-51.

10) S. Natsui, T. Sudo, T. Kikuchi, and R. O. Suzuki: *Electrochem. Commun.*, 2017, vol.81, pp. 43-47.

11) T. Takenaka, S. Akimura, and T. Morishige: *Electrochem.*, 2018,

vol. 86, pp. 179-83.

12) W. Xiao, X. Jin, Y. Deng, D. Wang, and G. Z. Chen: *J. Electroanal. Chem.*, 2010, vol. 639(1-2), pp. 130-140.

13) W. Xiao, X. Jin, Y. Deng, D. Wang, X. Hu, and G. Z. Chen: *ChemPhysChem*, 2006, vol. 7(8), 1750-1758.

14) Y. Deng, D. Wang, W. Xiao, X. Jin, X. Hu, and G. Z. Chen: *The J. Phys. Chem. B*, 2005, vol. 109(29), 14043-14051.

15) S. Natsui, T. Sudo, T. Kaneko, K. Tonya, D. Nakajima, T. Kikuchi, and R. O. Suzuki: *Sci. Rep.*, 2018, vol. 8, pp. 13114.

16) Y. Sakamura, M. Kurata, and T. Inoue: *J. Electrochem. Soc.*, 2006 vol. 153, pp. D31-D39.

17) H. Kuma, K. Ito, and M. Kawakami: *Tetsu-to-Hagane*, 1990, vol. 76, pp. 1656-63.

18) P. Lai, M. Hu, Z. Qu, L. Gao, C. Bai, T. Wang, S. Zhang, and G. Qiu, *Metall. Mater. Trans. B*, 2018, vol. 49, pp. 3403-3412.

19) K. S. Mohandas, and D. J. Fray: *Trans. Indian Inst. Met.*, 2004, vol. 57, pp. 579-92.

20) R. C. DeVries, and R. Roy: *Am. Ceram. Soc. Bull.*, 1954, vol. 33, pp. 370-72.

316 Captions List

317

318 Fig. 1 Titanium oxide electrode previously
319 prepared by heat treatment under air environment.
320 (a): Photos of the three, different-thickness
321 titanium oxide electrodes. (b): Scanning electron
322 microscope (SEM) image of the T2.0 electrode
323 cross-section. (c): X-ray diffraction (XRD) pattern
324 of electrodes before and after heat treatment.

325

326 Fig. 2. Cyclic voltammogram and corresponding
327 photographs of T7.5 titanium oxide electrode in
328 LiCl-KCl. Images were taken at a: -0.50V, b: -0.70V,
329 c: -1.00V, d: -1.10V, e:-1.30V, f:-2.50V, g: -2.45V,
330 h: -0.50V.

331

332 Fig. 3. Electro-reduction behavior of T2.0 and T7.3
333 TiO_2 electrodes observed by chronoamperometry (at
334 *E* = -2.75 V). (a): current-time curves, (b):
335 representative photographs of electrode.

336

337 Fig. 4. Electro-reduction behavior of T2.0 TiO_2
338 electrodes observed by chronoamperometry (at various
339 potentials). (a): voltage-time curves, (b):
340 representative photographs of electrode.